

Elliptic flow in intermediate energy heavy ion collisions and in-medium effects

Declan Persram and Charles Gale
Physics Department, McGill University
3600 University St., Montréal, QC, H3A 2T8, Canada
(October 31, 2018)

We investigate elliptic flow in heavy ion collisions at intermediate energies. In doing this, we implement and use a lattice-Hamiltonian model of the nuclear interaction and we also study the effect of in-medium nucleon-nucleon cross sections that follow consistently from the momentum-dependence of the nuclear mean field.

I. INTRODUCTION

Heavy ion collisions is an area of research which seeks to study physical systems under extreme conditions of density and temperature in experiments occurring in terrestrial laboratories. As such, it represents a rich and challenging field well worthy of intellectual pursuit and its study is important for a deep and a more complete understanding of Nature. At high energies, one goal of this program is to form and study a new state of matter which is a tantalizing prediction of QCD: the quark-gluon plasma [1]. At lower energies, the experimental and theoretical efforts have focused on the need to characterize and quantify the nuclear equation of state [2]. This physics also has an important role to play in the theory of supernovæ and that of neutron star properties [3]. It is that energy regime that we consider in this work.

In order to identify novel many-body features without ambiguity it is imperative to provide a realistic model of the nuclear reaction dynamics. An approach that has proven to be extremely successful is the Boltzmann-Uehling-Uhlenbeck (BUU) model of heavy ion collisions [4]. In BUU simulations, nucleons can suffer hard collisions and can also move on curved trajectories owing to interactions with the self-consistent mean field. The interaction term we use in this work is introduced and described in Refs. [5,6]. In connection with observables, a considerable amount of information on the nuclear equation of state and on nonequilibrium precursor phenomena is accessible through the measurement of global collective behaviour. A large body of work in intermediate energy nuclear collisions has been devoted to the measurement and to the theoretical calculation of both directed flow [7–10], and elliptic flow [11–13]. For reviews, see [14], and references therein.

Near the low end of the intermediate energy spectrum, some studies have put forward the possibility of observing experimental signatures of new phenomena. A good example is that of modified in-medium nucleon-nucleon cross sections [15–20]. Those would signal a departure from vacuum properties. While the confirmation of such manifestations would indeed be extremely interesting, one must keep in mind that such “new physics” issues must be addressed with an approach that incorporates all of the known physics in a computationally tractable model. Our goal in this paper is to first briefly describe such a model, and then to compare its results with experimental data. At the lower beam energies considered in this work, the problem of energy and momentum conservation in transport models is a pressing one. In addition, the momentum dependence of the nuclear mean field is an unavoidable feature, both from the point of view of theory and from that of experiment [21–24]. With those issues in mind, we use a momentum-dependent lattice Hamiltonian model as a solution of the BUU transport equation. This specific model has previously been used in [25], and provides for excellent energy and momentum conservation. A similar approach was developed in parallel in [26]. The momentum-independent lattice Hamiltonian method was first used in [27].

Our paper is organized as follows: the next section is a brief discussion of the momentum-dependent lattice Hamiltonian model. The following section introduces the self-consistent in-medium correction to the free-space nucleon-nucleon cross section as dictated by the functional momentum dependence that is observed in the nuclear mean field. Next, a comparison of model results with compiled and recent measurements of directed and elliptic flow in the range of laboratory bombarding energy $E_k/A : 25 \rightarrow 800$ MeV is performed. We then summarize and conclude.

II. THE MODEL

A. Lattice Hamiltonian solution of the mean field

In this work, we use the BUU transport model which characterizes the time evolution of a system of nucleons during the course of a collision of two heavy ions. The BUU equation reads:

$$\begin{aligned}
& \frac{\partial f(\vec{r}, \vec{p}, t)}{\partial t} + \nabla_{\vec{p}} h \cdot \nabla_{\vec{r}} f(\vec{r}, \vec{p}, t) - \nabla_{\vec{r}} h \cdot \nabla_{\vec{p}} f(\vec{r}, \vec{p}, t) \\
&= \int d^3 p_1 d\Omega' \left(v_{rel}^* \times \frac{d\sigma^*}{d\Omega'} \right) (f' f_1 \bar{f} \bar{f}_1 - f f_1 \bar{f}' \bar{f}'_1).
\end{aligned} \tag{2.1}$$

The left-hand side of (2.1) accounts for the time evolution of the semi-classical nucleon phase space distribution function f due to nucleon transport and mean field effects, and the right-hand side accounts for binary nucleon-nucleon collisions which also modify f . The nucleon single-particle Hamiltonian $h = t + u$, contains both the single particle kinetic energy and the mean field single particle potential. The starred quantities in the collision term represent in-medium values of the relative velocity and differential nucleon-nucleon scattering cross section respectively, and \bar{f} accounts for Pauli blocking [4].

For the nucleon-single particle potential, we adopt the momentum-dependent parameterization for nuclear matter used in [6], supplemented with symmetry and Coulomb terms

$$\begin{aligned}
u(\vec{r}, \vec{p}, \tau_3, t) &= A \left(\frac{\rho(\vec{r}, t)}{\rho_0} \right) + B \left(\frac{\rho(\vec{r}, t)}{\rho_0} \right)^\sigma + \frac{2C}{\rho_0} \int d^3 p' \frac{f(\vec{r}, \vec{p}', t)}{1 + \left(\frac{\vec{p} - \vec{p}'}{\Lambda} \right)^2} \\
&\quad - \tau_3 \frac{2D}{\rho_0} (\rho_n(\vec{r}, t) - \rho_p(\vec{r}, t)) + \frac{(\tau_3 + 1/2)}{4\pi\epsilon_0} \int d^3 r' \frac{\rho_p(\vec{r}', t)}{|\vec{r} - \vec{r}'|}.
\end{aligned} \tag{2.2}$$

This functional is amenable to computational applications and also incorporates nonequilibrium features [5,6]. The strong interaction part of the mean field is fixed by specifying the value of the parameters A, B, σ, C and Λ , neglecting the isospin and Coulomb terms. The parameter set from [6], deduced for symmetric nuclear matter, specifies: $A = -322.0$ MeV, $B = 352.5$ MeV, $\sigma = 12/11$, $C = 62.75$ MeV and $\Lambda = 1.58 p_f^0$ which gives $u(p = 0) = -72.4$ MeV, $u(p = p_f) = -51.4$ MeV and $u(p \rightarrow \infty) = +30.5$ MeV for a zero temperature equilibrium nuclear matter distribution at saturation density $\rho_0 = 0.16$ fm $^{-3}$. The zero temperature effective mass at the Fermi surface and nuclear matter compressibility for this parameterization are $m^*/m = 0.67$ and $K = 210$ MeV respectively. The charge-dependent part of the nucleon mean field is taken into account with the isospin and Coulomb contributions to the single particle potential, where τ_3 is the third component of isospin of the nucleon and ρ_n and ρ_p are the local neutron and proton densities, respectively. For the isospin part of the mean field, empirically it is found that $D = 34 \pm 4$ MeV. Furthermore, support for D ranging from 27–40 MeV is found from various phenomenological investigations [28, and Refs. therein]. We adopt the value of $D = 32$ MeV previously used in the context of simulations of heavy ion collisions [29–32]. The above parameterization of the mean field provides a good fit to the nuclear equation of state for both symmetric nuclear matter and pure neutron matter as calculated in [33,34] for a only slightly larger value of the nuclear compressibility. Note however that the exact high density behavior of the symmetry energy is still an open question that stems partly from the uncertainty in the high density many-body calculations [3], and partly from the different theoretical paradigms leading to the equation of state [35].

The nucleon dynamics are realized through the use of the lattice Hamiltonian [27] equations of motion, whereby the semi-classical nucleon phase space density for N_{ens} systems of A nucleons is projected onto a configuration space lattice with a finite grid constant δx . At lattice site α , the semi-classical phase space density reads:

$$f_\alpha(\vec{p}, t) = \frac{1}{N_{ens}} \sum_i^{A \times N_{ens}} R(\vec{r}_\alpha - \vec{r}_i(t)) \delta(\vec{p} - \vec{p}_i(t)) \tag{2.3}$$

With this, the lattice Hamiltonian equations of motion for particle i read:

$$\frac{\partial \vec{r}_i}{\partial t} = \frac{\vec{p}_i(t)}{(p_i(t)^2 + m^2)^{1/2}} + N_{ens} (\delta x)^3 \sum_\alpha R(\vec{r}_\alpha - \vec{r}_i(t)) \nabla_{\vec{p}_i} u_\alpha(\vec{p}_i, \tau_3^i, t) \tag{2.4}$$

$$\frac{\partial \vec{p}_i}{\partial t} = -N_{ens} (\delta x)^3 \sum_\alpha u_\alpha(\vec{p}_i, \tau_3^i, t) \nabla_{\vec{r}_i} R(\vec{r}_\alpha - \vec{r}_i(t)), \tag{2.5}$$

where $u_\alpha(\vec{p}_i, \tau_3^i, t)$ is the discretized form of (2.2), and R is the finite width configuration space nucleon form factor. In this work, we use $N_{ens} = 100$, $\delta x = 1.00$ fm and a quadratic form factor which provides for good energy and linear momentum conservation as shown in [36]. In one dimension, the form factor is defined as $R(x) = (3\delta x^2/4 - x^2)/\delta x^3$ for $0 \leq x \leq \delta x/2$, $R(x) = (3\delta x/2 - x)^2/2\delta x^3$ for $\delta x/2 < x \leq 3\delta x/2$ and $R(x) = 0$ for $3\delta x/2 < x$. The normalization factor of $1/N_{ens}$ in (2.3) and $1/\delta x^3$ and $1/2\delta x^3$ in R are chosen such that particle number is conserved. That is:

$$A = (\delta x)^3 \sum_{\alpha} \int d^3 p f_{\alpha}(\vec{p}, t), \quad (2.6)$$

at all times t . Note that the lattice Hamiltonian equations of motion (2.4) and (2.5) are derived from the *total* Hamiltonian H , and not the *single particle* Hamiltonian h , as is the case with the often-used test-particle method [4,27]. This work constitutes the first application (with Refs. [25] and [36]) of the lattice Hamiltonian approach with the interaction of Eq. (2.2) calculated fully dynamically. See also Ref. [37].

B. In-medium effects in nucleon collisions

For the calculation of the Uehling-Uhlenbeck collision term, we follow the cascade procedure outlined in [4] in conjunction with a Pauli blocking algorithm which distinguishes between protons and neutrons. However, the in-medium scattering cross section is calculated such that the functional dependence on momentum that is observed in the nuclear mean field is respected [36]. Fermi's Golden Rule gives an expression for the total free space nucleon-nucleon cross section in vacuum:

$$\sigma_{free} = \frac{2\pi V}{\hbar} \frac{D_f^{(0)}}{v_{rel}^{(0)}} |t_{fi}|^2, \quad (2.7)$$

where $v_{rel}^{(0)}$ and $D_f^{(0)}$ are the relative velocity of the colliding nucleons and density of final states for the two-nucleon scattering process respectively. Both of these quantities are expressed as the free space value. In matter, we write the total in-medium nucleon-nucleon cross as

$$\sigma^* = \frac{2\pi V}{\hbar} \frac{D_f^*}{v_{rel}^*} |t_{fi}^*|^2, \quad (2.8)$$

where the starred quantities represent in-medium values. Detailed many-body calculations offer support for $t_{fi}^* \sim t_{fi}$, as expected for low local densities and/or low energy collisions [38, and Refs. therein]. We follow this line of thought here. In [38], the in-medium cross-section is calculated as it is here, however a simplified momentum-dependence in the mean field potential was used. We rewrite the in-medium elastic scattering cross section as:

$$\sigma^* = \frac{v_{rel}^{(0)}}{v_{rel}^*} \frac{D_f^*}{D_f^{(0)}} \sigma_{free}. \quad (2.9)$$

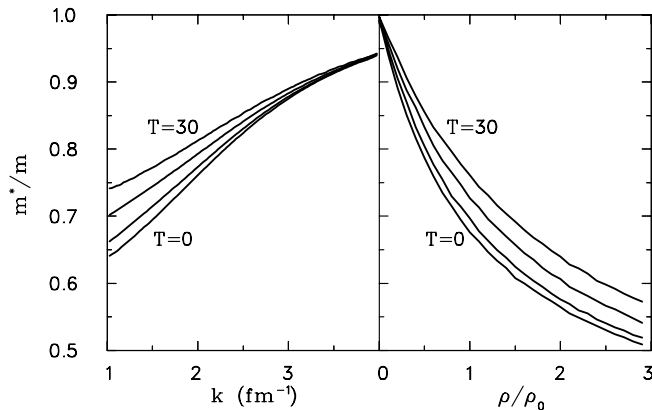


FIG. 1. Nucleon effective mass in equilibrium nuclear matter as a function of momentum at saturation density ρ_0 (left panel) and density at the Fermi surface (right panel) for temperatures of 0, 10, 20 and 30 MeV. In the above, $k = p/\hbar$.

We note that a closed form solution to (2.9) exists for an equilibrium nuclear matter distribution. In this case, the in-medium nucleon-nucleon total cross section reads:

$$\sigma^* = \left(\frac{m^*(\rho, p)}{m} \right)^2 \times \sigma_{free}, \quad (2.10)$$

where the nucleon effective mass m^* is defined as:

$$\frac{m^*(\rho, p)}{m} = \left(1 + \frac{m}{p} \frac{\partial u(\rho, p)}{\partial p} \right)^{-1}, \quad (2.11)$$

and we have replaced the \vec{r} dependence in u with a ρ dependence which is appropriate for an equilibrium nuclear matter distribution. Note that the density $\rho(\vec{r})$ is a constant in this case and it enters into the above relation self-consistently via the semi-classical phase space distribution function f (see, for example, Ref. [39]). In this work a modern and accurate parameterization of the nucleon-nucleon cross sections is used [40]. We show in figure 1 the ratio of the nucleon effective mass to the free mass as a function of momentum, density and temperature for an equilibrium nuclear matter distribution. As seen in the figure, the nucleon effective mass approaches the free mass in the high momentum, high temperature and low density limit as is expected from the many-body nature of this phenomenon.

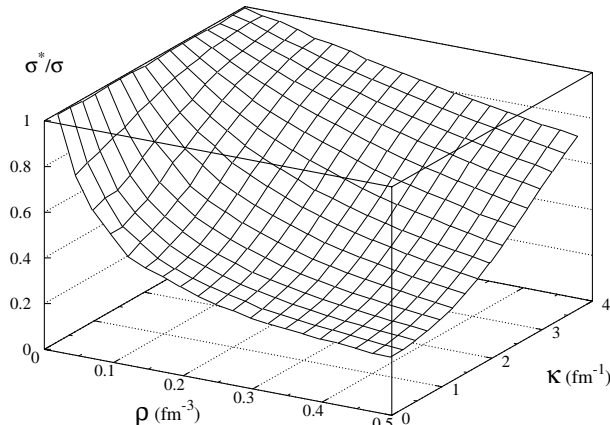


FIG. 2. Ratio of the in-medium to that of the free space nucleon-nucleon elastic scattering cross section for an equilibrium nuclear matter distribution at $T = 0$ MeV.

In figure 2 we show the ratio of the in-medium to that of the free space nucleon-nucleon total cross section as a function of both density and momentum for an equilibrium nuclear matter distribution at $T = 0$. Note that for momentum-independent mean field potentials, the effective mass is equal to the free mass and consequently, the in-medium cross section is equal to the free space cross section.

C. Dynamical effects in heavy ion collisions

We now wish to apply our model developed thus far to simulate the collision of two heavy ions. In this scenario, dynamical effects will generate a nuclear matter distribution that is in general not that of a zero temperature system. Furthermore, one also expects a nuclear matter distribution that is different from the equilibrium situation. In this case, one cannot use the zero temperature equilibrium closed form solution of (2.2) as given in [5]. Instead, (2.2), (2.4), (2.5) and (2.9) must be explicitly and dynamically calculated at all times during the collision process. In this work, we present the first results of the self-consistent calculation of (2.9) as applied to the dynamical collision of heavy ions.

In the initial stages of the collision of two heavy ions, large deviations from equilibrium will result in binary nucleon-nucleon centre of mass collision energies higher than that at later stages in the collision process. From figure 2 one can infer that initially, owing to the density and momentum-dependence in (2.10), the in-medium cross section will be larger at earlier stages in the collision compared to later times. In addition, one can also infer that higher centre of mass nucleus-nucleus collision energies will result in an in-medium cross section that is closer to the free space value. We illustrate this for a simulation of the head-on collision of two ^{209}Bi nuclei at laboratory bombarding energies of 25, 150, 500 and 1000 MeV/A in the left panel of figure 3. In this figure, we show the mean value of the in-medium nucleon-nucleon cross section for unblocked collisions as a function of time. We note that previous attempts to model

the in-medium nucleon-nucleon cross section have used a constant overall scaling factor [15,16,41]. Others have used a phenomenological density-dependent in-medium cross section of the form

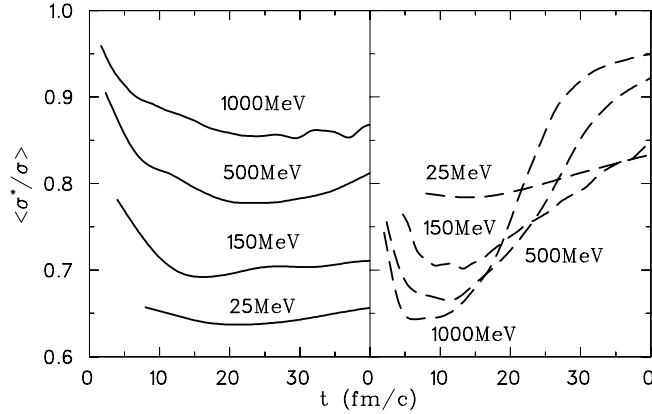


FIG. 3. Mean value of the ratio of the in-medium to that of the free space nucleon-nucleon scattering cross section for dynamical collisions of $^{209}\text{Bi}+^{209}\text{Bi}$ at laboratory bombarding energies per nucleon of 25, 150, 500 and 1000 MeV as a function of time. The left panel displays the results of the self-consistent calculation of (2.9) and the right panel shows the results of the phenomenological density-dependent ansatz given in (2.12) with $\alpha = 0.20$.

$$\sigma^* = (1 - \alpha\rho/\rho_0)\sigma_{free}, \quad (2.12)$$

where α is an adjustable parameter [17,18]. We show in the right panel of figure 3 that adoption of this simple ansatz results in an in-medium cross section that has considerably different behaviour from that of the self-consistent calculation. The self-consistent modification to the free space cross section in (2.9) effectively probes the shape of the momentum-dependent part of the single particle potential at all momenta. Such a detailed modeling is not possible with neither a constant scaling factor nor the density-dependent relation in (2.12). We will address the consequences of these differences in terms of elliptic flow in section III. Before we leave this section, we show in figure 4 a sample (250 events at each energy) of the values of the self-consistent in-medium cross section as a function of density for the $t : 10 \rightarrow 20 \text{ fm/c}$ time slice from figure 3 for all energies.

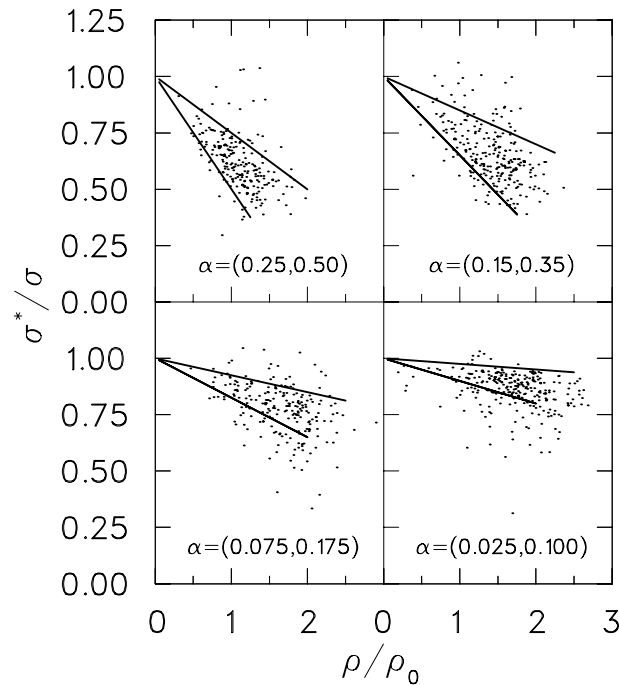


FIG. 4. Value of the self-consistent in-medium cross section for the $t : 10 \rightarrow 20 \text{ fm/c}$ time slice from figure 3 for all energies considered in that figure (scattered points). Moving from left to right and top to bottom, the panels are for energies of 25, 150, 500 and 1000 MeV. The solid lines represent the value of the in-medium cross section using (2.12) with various values of the parameter α .

Owing to the additional momentum-dependence in the in-medium cross section, we see that for a given density, the former can take on drastically different values. The solid lines in that figure indicate the value of the in-medium cross section that would be obtained by using the relation given in (2.12) for two different values of α . Again, we see that (2.12) clearly oversimplifies the in-medium result from (2.9).

To summarize, we note that the calculation of the self-consistent momentum (and density) dependent in-medium cross section indicates that the latter approaches the free space cross section for high centre of mass nucleus-nucleus collision energies and steadily decreases with centre of mass nucleus-nucleus collision energies. Also, at early stages in the nucleus-nucleus collision, non-equilibrium effects results in an in-medium cross section that is closer to the free space value then compared to later times in the nucleus-nucleus collision process. This implementation of a self-consistent, momentum-dependent, BUU transport model represents a considerable numerical challenge. Efforts to develop algorithms in a parallel architecture are under way.

III. COLLECTIVE EFFECTS

A. Directed Flow

One of the often discussed signatures of collective motion in heavy ion collisions is the directed flow [7]. Typically, the projection into the reaction plane of the transverse momenta of the reaction products is plotted against the rapidity, resulting in the well known ‘‘S-shaped’’ plot. The directed flow is obtained by taking the slope of this plot at mid-rapidity. Specifically, one fits the flow plot with:

$$\frac{d \langle p_x \rangle}{dy} = a_1 + a_2 y + a_3 y^3, \quad (3.1)$$

where the rapidity fit interval is taken to be $|y| < y_{proj}$, and y_{proj} is the initial projectile rapidity. In this case, the flow F is given by the value of a_2 in (3.1). Often, a narrow mid-rapidity region is selected, and (3.1) is used to fit the flow, with $a_3 = 0$. Some recent flow data from the FOPI collaboration [42] is shown in figure 5.

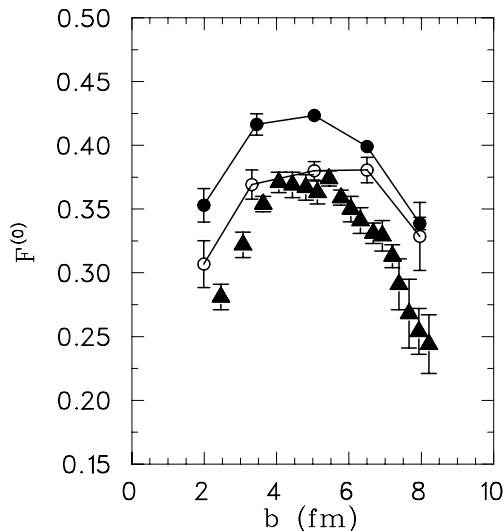


FIG. 5. Directed flow $F^{(0)}$ as a function of impact parameter for Au+Au collisions at 400 MeV/A. The measured points [42] shown by triangles, are obtained using a coalescence model as described in the text. The results from the BUU calculations are shown by the solid and open circles for a free space and in-medium cross section from (2.9) respectively. The BUU calculations are shown for all protons at mid-rapidity. The curves are drawn to guide the eye.

In this figure, the directed flow for Au+Au collisions at 400 MeV/A is shown as a function of impact parameter. The experimental data in this plot was obtained by using a coalescence model which weights all detected fragments by its measured charge [13]. We also show in this figure the results of our BUU simulations with a free space nucleon-nucleon cross section, and the in-medium cross section given in (2.9). Here, the normalized flow $F^{(0)} = F \times (y_{proj}/p_{proj})_{CM}$ is used. The coalescence-invariant prescription was developed to enable direct comparisons with transport models such as the BUU. All the BUU results were obtained by using (3.1) with and without $a_3 = 0$. For the $|y_n| = |y/y_{proj}| < 0.45$

cut, we find the two methods to be within one standard deviation of each other. Qualitatively, we find that both the free space and in-medium simulations predict the observed maximum in the flow magnitude for intermediate impact parameters. More quantitatively, we find the free space cross section over-predicts the flow magnitude for all impact parameters. The calculations with the in-medium cross section however, are generally in good agreement with the data at all impact parameters.

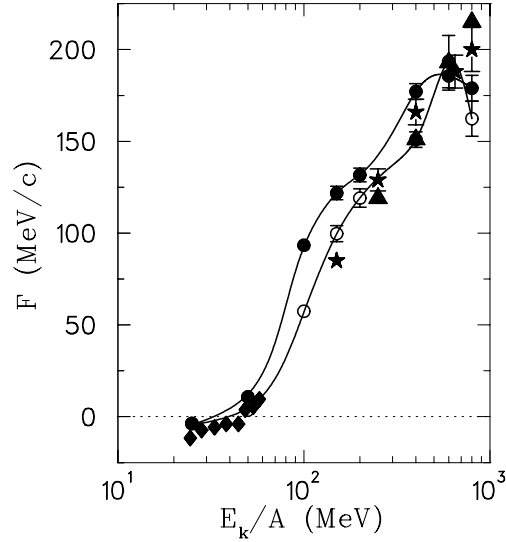


FIG. 6. Directed flow excitation function for Au+Au collisions. The measured points [9,44] shown by the triangles and stars are for fragments of charge $Z = 1, 2$. The measured points [43] shown by the diamonds are for fragments of charge $Z = 2$. The BUU results (circles) are as in figure 5 and are impact parameter averaged from $3.5 \text{ fm} < b < 6.5 \text{ fm}$ for $E_k/A \geq 100 \text{ MeV}$ at rapidity $-0.19 < y_n < +0.29$. For $E_k/A < 100 \text{ MeV}$, $\hat{b} < 0.39$ at rapidity $|y_n| < 0.5$, fm as is also the case with the measured points shown by the diamonds. The curves are drawn to guide the eye.

The directed flow excitation function also provides a means by which comparisons of measured signals to model calculations may be performed. With this in mind, we show in figure 6 a compilation of data near the balance energy [43] for central impact parameters and charge $z = 2$ fragments and for semi-central impact parameters at $E_k/A : 150 \rightarrow 800 \text{ MeV}$ [9,44] for charge $z = 1, 2$ fragments. The BUU results for the central impact parameters are shown for $|y_n| < 0.5$ and $\hat{b} = b/b_{max} < 0.39 \text{ fm}$ and for $-0.19 < y_n < +0.29$ and $(3.5 < b < 6.5) \text{ fm}$ for the semi-central impact parameters. To compare our BUU results with the measured fragment flow, free nucleons are omitted from the flow analysis; see Ref. [36] for a discussion.

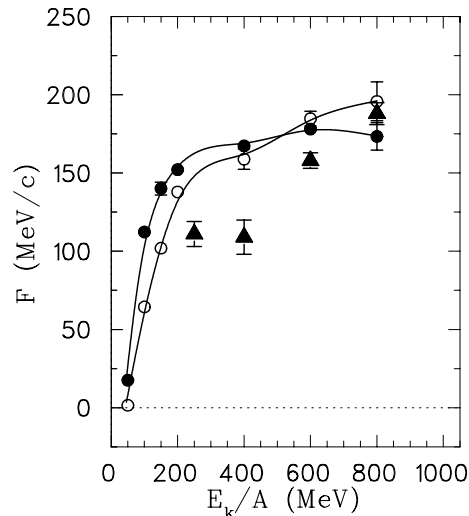


FIG. 7. Same as figure 6, but for free protons only. The measured points [9] are shown by triangles and the BUU results (circles) are as in figure 5. The curves are drawn to guide the eye.

For the entire energy range probed here, we find that the calculations employing the in-medium nucleon-nucleon cross section result in a reduced value of the directed flow as compared with the free space cross section. From this figure, we find the in-medium result to be in better agreement with the data. A more stringent test of the model in terms of the directed flow is shown in figure 7. In this figure, the data for free protons [9] is shown along with the model predictions for free protons. The figure indicates that the predicted directed flow over-estimates the observed value. We point out however, that the coalescence-invariant comparison in figure 5 with the more recent data is in better agreement with the model calculations.

B. Elliptic Flow

We now turn to comparisons of the measured elliptic flow with our BUU model. The elliptic flow is a measure that quantifies the azimuthal anisotropy of the momentum distribution. Specifically, we fit the azimuthal distribution of nucleons about the reaction plane with a Fourier expansion of the form:

$$\frac{dN}{d\phi} = p_0 (1 + 2p_1 \cos(\phi) + 2p_2 \cos(2\phi)), \quad (3.2)$$

where the ellipticity coefficient p_2 depends on the in-plane and out-of-plane flow amplitudes. In addition, the anisotropy ratio is defined by: $R_n = (1 - 2p_2)/(1 + 2p_2)$. A ratio R_n larger than unity signals a preferred out-of-plane emission.

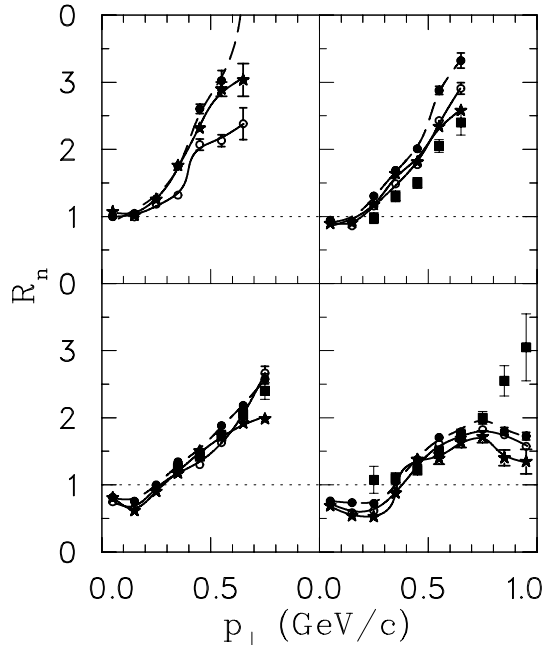


FIG. 8. Mid-rapidity ($|y_n| < 0.15$) free-proton anisotropy ratio for Bi+Bi collisions at incident laboratory bombarding energies of $E_k/A = 200, 400, 700$ and 1000 MeV moving left to right and top to bottom. The measured points [46] are shown by the squares. The BUU results are for a free space cross section (solid circles), density-dependent in-medium cross section (stars) from (2.12) and self-consistent in-medium cross section (open circles) from (2.9). The impact parameter for all cases is $\hat{b} \sim 0.65$. There are no data points available at 200 MeV. The curves are drawn to guide the eye.

In [45] it was shown that BUU calculations of the elliptic flow for a Bi+Bi system with a momentum-dependent nuclear mean field favoured a nucleon effective mass of $m^*/m \sim 0.6 - 0.7$. We show in figure 8, the results that we obtain for BUU calculations with the mean field in (2.2) of effective mass $m^*/m = 0.67$, for both a free space cross section and separately, the in-medium cross sections obtained with equations (2.9) and (2.12). The figure indicates that adoption of the self-consistent correction to the free space cross section is significant for the anisotropy ratio at the lower energies only (200 and 400 MeV/A). For the higher bombarding energies, the self-consistent result does not differ significantly from the free space result. Since the in-medium effect from (2.9) probes the shape of the momentum-dependence in the mean field it is more effective for lower bombarding energies, with many nucleon-nucleon collisions

occurring near the Fermi surface where the momentum-dependence is steepest. At high bombarding energies, the nucleon-nucleon collisions occur far from the Fermi surface where the momentum-dependence in the mean field is relatively flat, and as such, the correction to the free space cross section is small. The experimental results are from [46]. Unfortunately there are no data at the lower energy, where the differences in theoretical results are the largest.

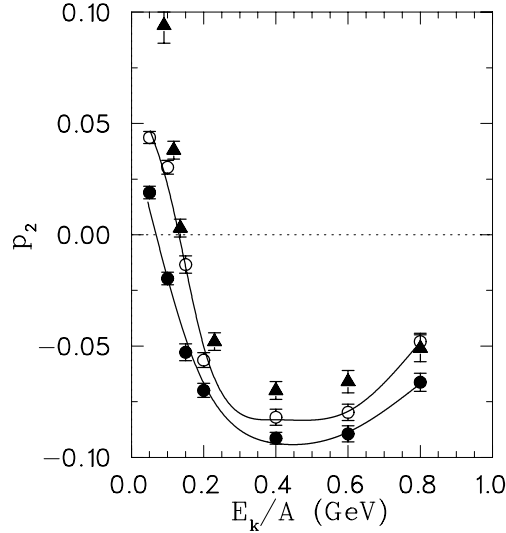


FIG. 9. Excitation function for the ellipticity coefficient for Au+Au collisions. The measured points [47] shown by the triangles are for fragments of mass $A = 1, 2, 3$, and are for an impact parameter range of $b : 5.3 \rightarrow 7.3$ fm. The BUU results (circles) are as in figure 5 and are shown for an impact parameter of $b = 6.5$ fm for all mid-rapidity nucleons. Mid-rapidity particles are selected with a $|y_n| < 0.1$ cut. The curves are drawn to guide the eye.

We now turn to the elliptic flow excitation function for Au+Au recently measured by the FOPI collaboration [47]. In figure 9, we show the ellipticity coefficient measured for fragments with $A = 1, 2, 3$ along with the appropriate BUU result. We find that both parameterizations of the nucleon-nucleon cross section (free space and in-medium result from (2.9)) are able to qualitatively reproduce the experimental trend. Quantitatively, the calculation with the in-medium cross-section is better able to reproduce the measured signal.

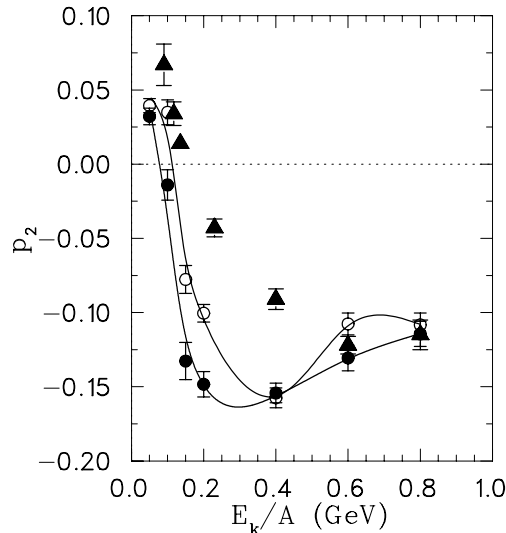


FIG. 10. Same as figure 9 but for high transverse momentum protons only ($p_{\perp}^{(0)} > 0.8$). The measured points are taken from [47] and are for an impact parameter range of $b : 5.3 \rightarrow 7.3$ fm. The BUU results (circles) as in in figure 5 and are shown for free protons at $b = 6.5$ fm. Mid-rapidity particles are selected as in figure 9. The curves are drawn to guide the eye.

We note that the ellipticity parameter is calculated in a frame where the principle axis of the momentum ellipsoid coincides with the beam axis. A more stringent test of the model is shown in figure 10 where the ellipticity coefficient

for free protons with transverse momenta $p_{\perp}^{(0)} > 0.8$ only, is plotted as a function of incident bombarding energy. Note that $p_{\perp}^{(0)} \equiv p_{\perp}/p_{beam}$. From this figure, we find that the elliptic flow in the energy range ($150 < E_k/A < 600$) MeV is over-predicted by the model. This agrees with figure 8, where we see that the magnitude of the elliptic flow is over-predicted at high transverse momentum. This identifies the phase space areas where the BUU seems to perform perhaps less satisfactorily. However there, the phase space distribution functions are small and therefore those regions do not contribute importantly to the momentum-integrated observables. This is seen in our results as well as in the experimental data. This observation however represents valuable information for future theoretical developments.

IV. CONCLUSION

In summary, we have shown for the first time the effect of the parameter-free self-consistent calculation of the nucleon-nucleon in-medium scattering cross section in BUU calculations of both directed and elliptic flow from $E_k/A : 25 \rightarrow 800$ MeV. Our results indicate that, globally, the in-medium cross section better describes the flow data than with the free space cross section. In addition, the self-consistent calculation of the in-medium cross section results in a value of the latter that is less than the free space cross section for low bombarding energies and approaches the free space cross section at high bombarding energies. While in some sense transport models utilizing vacuum cross sections are a well-defined low-density approach, there is still some work to be done to formulate and use a totally self-consistent many-body transport theory. For example, one needs to generalize to the coupled set of transport equations that include all additional degrees of freedom [48]. The work in this direction is continuing.

ACKNOWLEDGMENTS

This work is supported in part by the Natural Sciences and Engineering Research Council of Canada and in part by the Fonds FCAR of the Québec government. One of us (D.P.) is happy to acknowledge the financial support of McGill University through the Alexander McFee Memorial Fellowship.

-
- [1] See, for example, *Proceedings of the 15th. International Conference on Ultrarelativistic Nucleus-Nucleus Collisions (Quark Matter 2001)*, Nucl. Phys. **A** in press, and references therein.
 - [2] See *Proceedings of the Sixth International Conference on Nucleus-Nucleus Collisions* Nucl. Phys. **A629** (1998), and references therein.
 - [3] See, for example, Madappa Prakash, Ignazio Bombaci, Manju Prakash, Paul J. Ellis, James M. Lattimer, and Rolland Knorren, Phys. Rep. **280**, 1 (1997), and references therein.
 - [4] G. F. Bertsch and S. Das Gupta, Phys. Rep. **160**, 189 (1988).
 - [5] G. M. Welke, M. Prakash, T. T. S. Kuo, S. Das Gupta and C. Gale, Phys. Rev. **C38**, 2101 (1988).
 - [6] Jianming Zhang, Subal Das Gupta and Charles Gale, Phys. Rev. **C50**, 1617 (1994).
 - [7] P. Danielewicz and G. Odyniec, Phys. Lett. **B157**, 146 (1985).
 - [8] H.H. Gutbrod, A.M. Poskanzer, and H.G. Ritter, Rep. Prog. Phys. **52**, 1267 (1989).
 - [9] M.D. Partlan *et al.*, Phys. Rev. Lett. **75**, 2100 (1995).
 - [10] F. Haddad, F. Sébille, M. Farine, V. de la Mota, P. Schuck and B. Jouault, Phys. Rev. **C52**, 2013 (1995).
 - [11] H. Gutbrod, K. H. Kampert, B. Kolb, A. M. Poskanzer, H.G. Ritter and H.R. Schmidt, Phys. Lett. **B216**, 267 (1989).
 - [12] Jean-Yves Ollitrault, Phys. Rev. **D46**, 229 (1992).
 - [13] M. B. Tsang *et al.*, Phys. Rev. **C53**, 1959 (1996).
 - [14] W. Reisdorf and H. G. Ritter, Ann. Rev. Nucl. Part. Sci., **47**, 663 (1997); Norbert Herrmann, Johannes P. Wessels, and Thomas Wienold, *ibid*, **49**, 581 (1999).
 - [15] G. F. Bertsch, W. G. Lynch and M. B. Tsang, Phys. Lett. **B189**, 384 (1987).
 - [16] C. A. Ogilvie *et al.*, Phys. Rev. **C42**, 10 (1990).
 - [17] G. D. Westfall *et al.*, Phys. Rev. Lett. **71**, 1986 (1993).
 - [18] Dietrich Klakow, Gerd Welke and Wolfgang Bauer, Phys. Rev. **C48**, 1982 (1993).
 - [19] V. de la Mota, F. Sébille, M. Farine, B. Remaud and P. Schuck, Phys. Rev. **C46**, 677 (1992).
 - [20] A. Hombach, W. Cassing and U. Mosel, Eur. Phys. J. **A5**, 77 (1999).
 - [21] B. Friedmann and V. R. Pandharipande, Phys. Lett. **B100**, 205 (1981).

- [22] R. Maffiet, *Prog. Part. Nucl. Phys.* **21**, 207 (1988).
- [23] J. P. Jeukenne, A. Lejeune and C. Mahaux, *Phys. Rep.* **25c**, 85 (1976), and references therein.
- [24] L. P. Csernai, George Fai, C. Gale and Eivind Osnes, *Phys. Rev.* **C46**, 736 (1992).
- [25] D. Persram and C. Gale in: *AIP conference proceedings: Toward the Theory of Everything: MRST'98*, eds. J.M. Cline, M.E. Knutt, G.D. Mahlon and G.D. Moore (AIP, Woodbury, New York, 1998) p.227
- [26] P. Danielewicz *et al.*, *Phys. Rev. Lett.* **81**, 2438 (1998).
- [27] R. J. Lenk and V. R. Pandharipande, *Phys. Rev.* **C39**, 2242 (1989).
- [28] C. H. Lee, T. T. S. Kuo, G. Q. Li and G. E. Brown, *Phys. Rev.* **C57**, 3488 (1998).
- [29] M. B. Tsang, G. F. Bertsch, W. G. Lynch and M. Tohyama, *Phys. Rev.* **C40**, 1685 (1989).
- [30] B.-A. Li and S. J. Yennello, *Phys. Rev.* **C52**, 1746 (1995).
- [31] Feng-Shou Zhang, Lie-Wen Chen and Zhi-Yuan Zhu, *Eur. Phys. J.* **A9**, 149 (2000).
- [32] J.-Y. Liu, W.-J. Guo, S.-J. Wang, W. Zuo, Q. Zhao and Y.-F. Yang, *Phys. Rev. Lett.* **86**, 975 (2001).
- [33] A. Akmal and V. R. Pandharipande, *Phys. Rev.* **C56**, 2261 (1997).
- [34] A. Akmal, V. R. Pandharipande and D. G. Ravenhall, *Phys. Rev.* **C58**, 1804 (1998).
- [35] J. M. Lattimer and M. Prakash, *Astrophys. J.* **550**, 426 (2001); M. Prakash, private communication.
- [36] D. Persram, Ph.D. thesis, McGill University, (2001).
- [37] A. B. Larionov *et al.*, *Phys. Rev.* **C62**, 064611 (2000).
- [38] V. R. Pandharipande and S. C. Pieper, *Phys. Rev.* **C45**, 791 (1992).
- [39] C. Gale, G. M. Welke, M. Prakash, S. J. Lee and S. Das Gupta, *Phys. Rev.* **C41**, 1545 (1990).
- [40] J. Cugnon, D. L'Hôte, and J. Vandermeulen, *Nucl. Instrum. Methods* **B111**, 215 (1996).
- [41] Hong Ming Xu, *Phys. Rev. Lett.* **67**, 2769 (1991).
- [42] F. Rami *et al.*, *Nucl. Phys.* **A646**, 367 (1999).
- [43] D. J. Magestro *et al.*, *Phys. Rev.* **C61**, 021602 (2000).
- [44] H. A. Gustafsson *et al.*, *Mod. Phys. Lett.* **3**, 1323 (1988).
- [45] P. Danielewicz, *Nucl. Phys.* **A673**, 375 (2000).
- [46] D. Brill *et al.*, *Z. Phys.* **A355**, 61 (1996).
- [47] A. Andronic *et al.*, *Nucl. Phys.* **A661**, 333 (1999).
- [48] Bao-An Li and Wolfgang Bauer, *Phys. Rev. C* **44**, 450 (1991); W. Cassing and E. L. Bratkovskaya, *Phys. Rep.* **308**, 65 (1999).